Extended cut-off wavelength nBn detector utilizing InAsSb/InSb digital alloy absorber

A. Soibel, D. Z. Ting, C. J. Hill, Anita M. Fisher, Linda Hoglund, Sam. A. Keo, and Sarath D. Gunapala

Jet Propulsion Laboratory, California Institute of Technology, 4800 Oak Grove Dr., Pasadena, CA, 91109, USA

Abstract

We investigated a novel approach to extend a cut-off wavelength of Sb-based nBn detectors. We incorporated a series of single InSb monolayer into InAsSb bulk that allowed to realize a digital alloy absorber with an extended cut-off wavelength of λ = 4.6 μm at T = 200 K. The cut-off wavelength extension to 4.6μm is technologically important for realization of detectors covering CO_2 absorption line at 4.26μm

.

Keywords: infrared detectors, mid-wavelength infrared (LWIR), InAsSb/InSb photodiodes, nBn

1. INTRODUCTION

Mid-wavelength infrared (MWIR) detectors covering 3-5μm atmospheric transmission windows are of great interest for NASA Earth Science missions. The recently demonstrated nBn or XBn barrier photodetectors[1,2,3] offer many advantages for realization of high performance infrared imagers (IR). In these detectors, a wide band gap barrier layer, which is sandwiched between the top contact and the absorber layers, blocks the flow of majority carriers (electrons), but not of minority carriers. This architecture offers advantages of reduced dark current resulting from suppressed Shockley-Read-Hall (SRH) recombination process[4] and of planar processing. However, the barrier photodetectors require the appropriate band alignment between absorber and the barrier, as well as lattice-matching to a suitable substrate. This limits the detector implementation by the available choice of the barrier and absorber materials. So far, the most successful approach for implementation of high performance barrier photodetectors is to utilize an InAsSb/AlAsSb absorber-barrier combination but the cut-off wavelengths in this design is limited to about λ_c = 4 μm.

In our research we investigated a novel approach to extend a cut-off wavelength of Sb-based nBn detectors.[5] We incorporated a series of single InSb monolayer into InAsSb bulk that allowed to realize a digital alloy absorber with an extended cut-off wavelength of λ = 4.6 μm at T = 200 K. The cut-off wavelength extension to 4.6μm is technologically important for realization of detectors covering CO_2 absorption line at 4.26μm. At the same time, the constructed digital alloy InAsSb/InSb is a fascinating material system that has an energy bandgap smaller that the random allow with the same material composition. The developed nBn detectors with 2μm thick absorber showed a temperature independent quantum efficiency $QE \approx 0.45$ for back-side illumination without antireflection coating. The dark current density was j_d = 5×10^{-6} A/cm^2 at T = 150K, and increased to $j_d = 2 \times 10^{-3}$ A/cm^2 at T = 200K. At temperatures of T = 150 K and below, the demonstrated photodetectors operate in background limited (BLIP) mode, with detectivity $D^*(\lambda)$=3-6 x 10^{11} (cmHz$^{0.5}$/W) for the background temperature of 300K, and f/2 field of view.

*Alexander.Soibel@jpl.nasa.gov; phone 818 393 0225; fax: 818 393 4540;

2. DETECTOR DESIGN, GROWTH AND FABRICATION

The photodetector demonstrated in this work is based on nBn architecture with an absorber layer utilizing InAsSb/InSb digital alloy (Fig. 1). The digital alloy is constructed by the incorporation of a single InSb monolayer after every 14 monolayers of $InAs_{0.92}Sb_{0.08}$. For this nomimal structure, the calculated cutoff wavelengths at 80K and 160K are 4.5µm and 4.79µm. The calculated 100K hole conductivity effective mass along the growth direction is ~1.34 m_0, which is approximately 5 time higher than that of the bulk InAsSb. The barrier photodetector structures were grown in a Veeco Applied-Epi Gen III molecular beam epitaxy chamber on low n-type doped ($1\times10^{17}cm^{-3}$) GaSb substrate. The absorbing layer was unintentionally doped, and n-type carrier concentration of n_{abs} = 5×10^{14} cm^{-3} was later measured with capacitance-voltage measurement system. The barrier layer was unintentionally doped and estimated to have a residual p-type carrier concentration of ~ $10^{15}cm^{-3}$. This sample exhibited high-quality X-ray diffraction patterns and good lattice mismatch (2190 ppm).

Single pixel square detectors with pixel side sizes ranging from 150µm to 1000µm were fabricated by wet etching. Detectors were partially delineated, with an etch depth of ~0.6 µm (~0.4 µm into the absorber) and the ground contact was defined by etching into the bottom contact layer. The detector top and ground Ti/Pt/Au metal contacts were deposited by evaporation and a lift-off process. The detectors were mounted for back-side illumination and wire-bonded to ceramic leadless chip carrier (LCC).

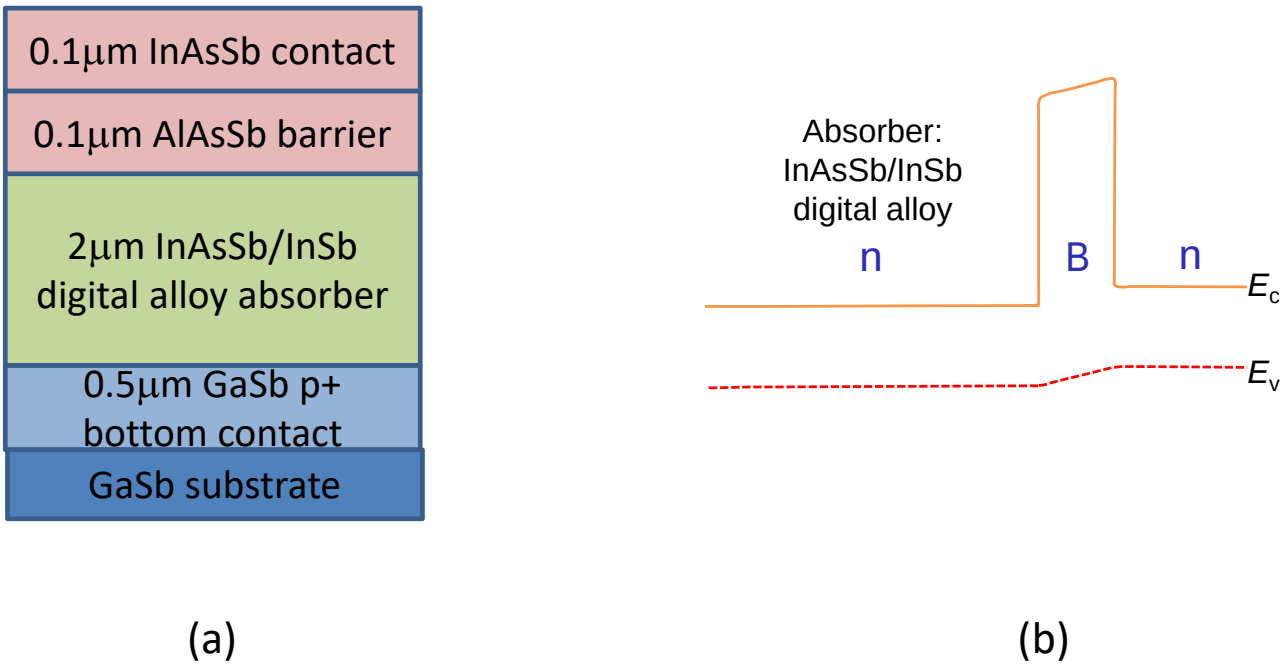

Figure 1. (a) Growth sequence of the nBn photodetector which consists of a 2 µm thick InAsSb/InSb absorber followed by a 0.1 µm $AlAs_{0.1}Sb_{0.9}$ barrier and a 0.1 µm $InAs_{0.915}Sb_{0.085}$ top contact (b) Schematic energy band diagram of nBn detector.

3. OPTICAL TESTS

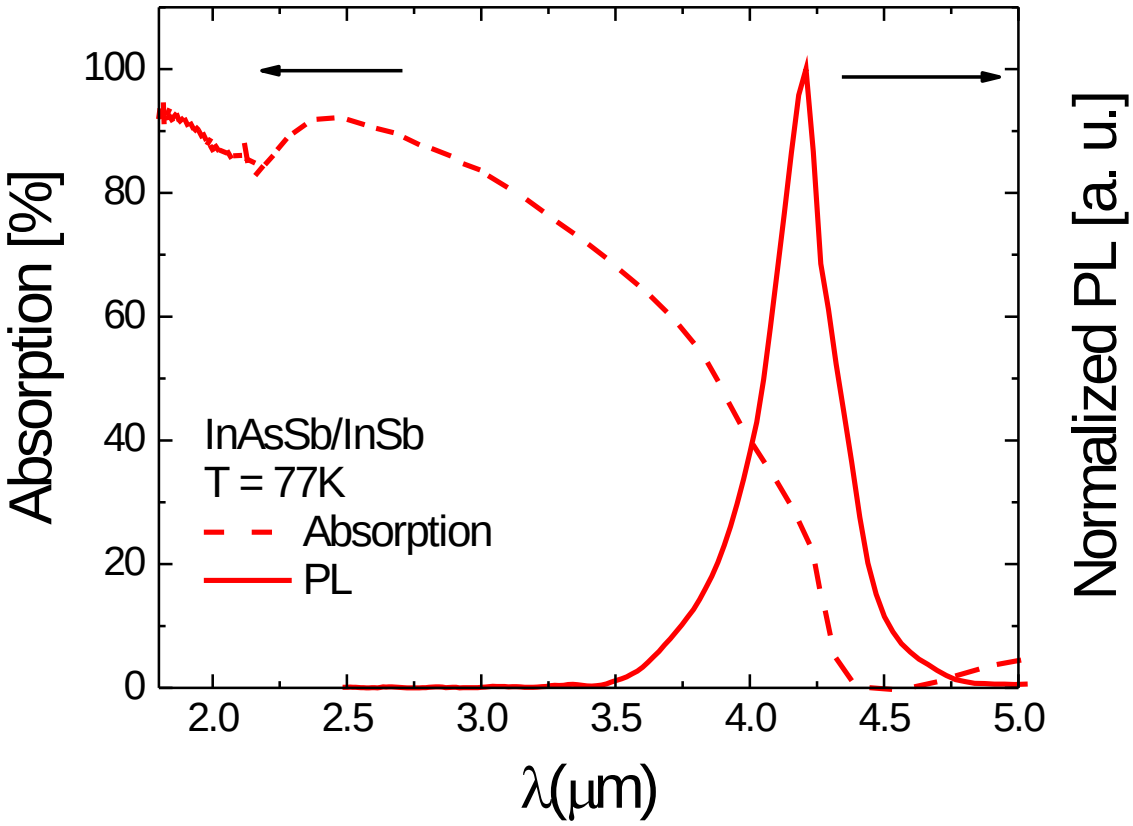

Figure 2. (Left axis) Absorption of 2 μm thick InAsSb/InSb absorber. (Right axis) Normalized photoluminescence intensity for InAsSb/InSb digital alloy.

We measured photoluminescence (PL) spectrum of the digital alloy as shown in Figure 2. At T = 77K, the digital alloy exhibits PL peak λ_{PL}^{da} = 4.21μm compared to the λ_{PL}^{bulk} = 3.79μm of $InAs_{0.915}Sb_{0.085}$ bulk material (not shown). The measured λ_{PL}^{da} is in fair agreement with the calculated cut-off wavelength. The absorption spectrum of the 2μm thick digital alloy absorber at T = 77 K is shown in Figure 2. Absorption is α = 70% and the absorption coefficient is α_c = 2900 cm^{-1} at λ = 3.4 μm. We measured minority carrier lifetime using optical modulation response technique[6] (Fig. 3). The minority carrier lifetime, τ_{da}, in the digital alloy at T = 77 K, was τ_{da} = 500 ns. The radiative recombination time τ_r = 400 ns, which was estimated from the absorption spectrum and the measured carrier concentration,[7] is close to the experimentally measured lifetime. It indicates that the radiative recombination controls the minority carrier lifetime in this sample at T = 77 K. In reference, the minority carrier lifetime in $InAs_{0.915}Sb_{0.085}$ bulk material was found to be τ_{bulk} = 300 ns for carrier concentration of n = 1-2 x10^{15} cm^{-3}.[8]

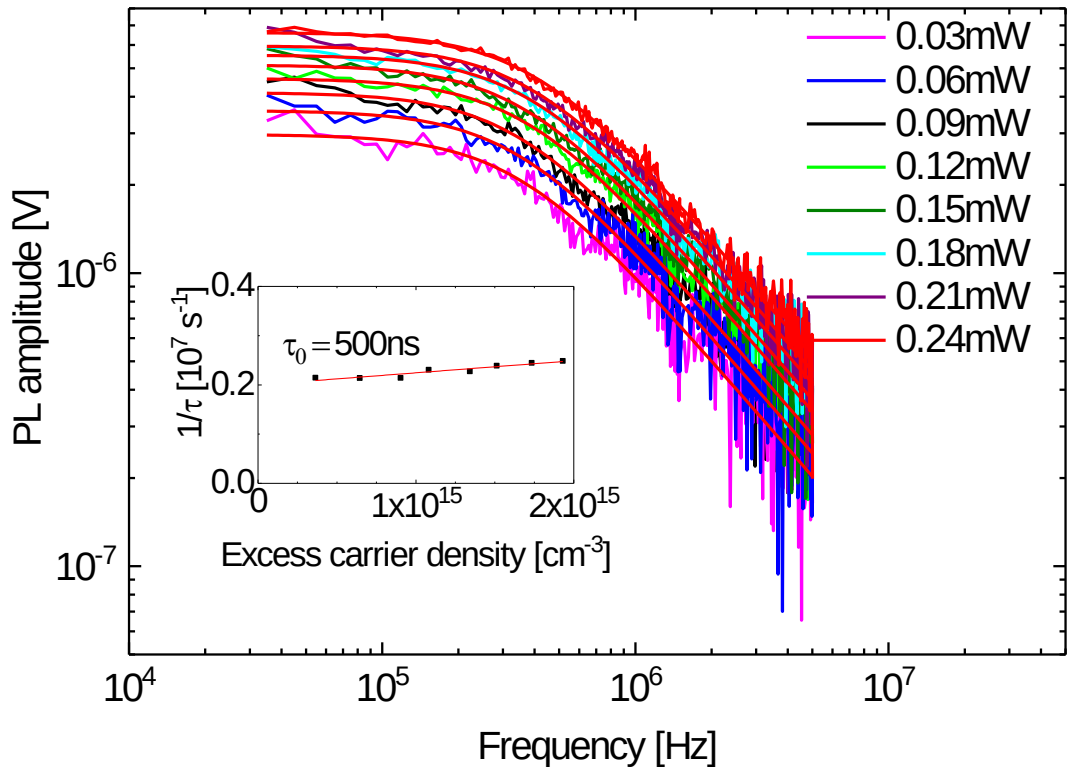

Figure 3. PL frequency response curves measured for a thick InAsSb/InSb superlattice at 77K for different continuous wave excitation powers. (Inset) Inverse carrier lifetime versus excess carrier density at 77K is plotted. An estimate of the minority carrier lifetime of 500 ns is obtained from the intersection of the linear fit of the inverse lifetime and the y-axis.

4. SPECTRAL TEST

Figure 4 shows the spectral response of backside-illuminated digital alloy nBn photodetector without antireflection (AR) coating in the temperature range T = 77 – 250 K. The transmission of the GaSb substrate used for the growth of these devices was found to be higher than >95% for $\lambda < 6\mu m$ (not shown) so substrate transmission does not affect the photodetector response noticeably. The measured photoresponse is for a double-pass configuration since IR light partially transmitted by the absorber is reflected back by the top contact. The maximum quantum efficiency is $QE^{max} \approx 0.5$ and does not change with temperature in the temperature range T = 77 – 250 K. The cut-off wavelengths, λ_c, which is defined as $QE(\lambda_c) = 0.5\ QE^{max}$, changes from λ_c = 4.34 μm at T = 77 K to λ_c = 4.77 μm at T = 250 K.

Figure 5 shows the QE at λ = 3.4 μm vs applied bias in the temperature range T = 77 – 200 K. At T = 77 K, the device turn-on bias, V_{on}, is less than 50 mV, which indicates good valence band alignment between the barrier and absorber. The turn-on bias increases with temperature to about V_{on} = 150 mV at T = 250 K. This bias increase with temperature is similar to what was observed in InAsSb bulk nBn[9] and can be attributed to band-bending effects.[10] After photodetector is completely turned on, QE does not change with applied bias and temperature. We can estimate the double pass quantum efficiency from the absorption by using the expression $QE_{est} = (1-R)(\alpha + \alpha(1-\alpha))$, where α is a single-pass abosrption and R = 0.34 is the reflectance of GaSb substrate (refractive index n = 3.8). The estimated quatntum efficiency, $QE_{est} \approx 0.6$ at λ=3.4 μm, is very close to the measured $QE^m \approx 0.5$. This shows that the diffusion length in these devices exceeds the abosrber thickness, d = 2 μm, in the temperature range T = 77 – 250 K.

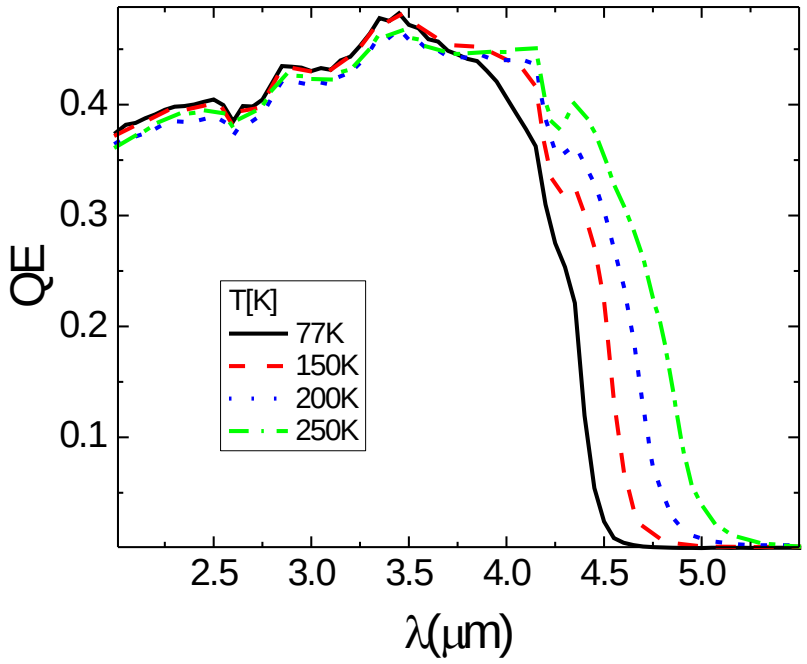

Figure 4. Detector responsivity Quantum Efficiency, QE_{resp}, in the temperature range T = 77 – 250 K.

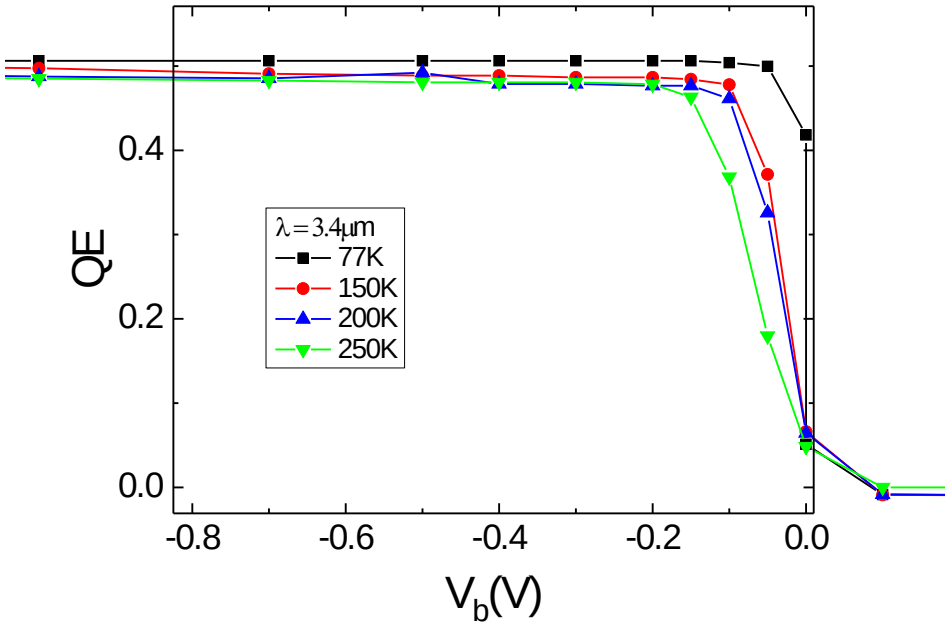

Figure 5. Detector turn-on bias, which is defined as bias at which detector reaches 90% of maximal Quantum Efficiency, vs. temperature.

5. DARK CURRENT TEST

The dark current density vs. applied bias at different operating temperatures is shown in Figure 6 for a 500 μm square device. The dark current density is $j_d = 5 \times 10^{-6}$ A/cm^2 at V_b = -0.1 V and T = 150 K, and increases to $j_d = 2 \times 10^{-3}$ A/cm^2 at T = 200 K. Neither the lateral current collection due to a partial pixel delineation nor the surface leakage current are noticeable in the dark current vs. perimeter/area ratio graph (not shown). The observed negligible lateral collection is an indication of a large ratio of pixel size to lateral diffusion length. We performed Arrhenius analysis of the dark current at applied bias V_b = -0.1V. In the temperature range of T = 150 – 250 K, the temperature dependence of dark current is well approximated by the expression for the diffusion dark current $j_{diff} \sim T^3 \exp(-Eg/k_BT)$ with an activation energy of E_{fg} = 0.288 meV (λ_{fg} = 4.3μm), which is derived from the data fit, and is very close to the superlattice bandgap value Eg = 0.294 meV estimated from the PL peak. At temperatures below 150K, the activation energy decrease indicates a larger contribution of generation-recombination (g-r) and tunneling processes into the dark current. Also, transition from the diffusion limited to g-r and tunneling dominated regimes is clearly visible from the dark current dependence on the applied bias (Figure 6). At temperatures above 150K and low applied biases, the dark current exhibits a flat dependence on the applied bias consistent with the diffusion dark current. At lower temperatures and higher biases, the dark current starts first to exhibit a weak and then a strong bias dependence consistent with g-r and tunneling regimes.

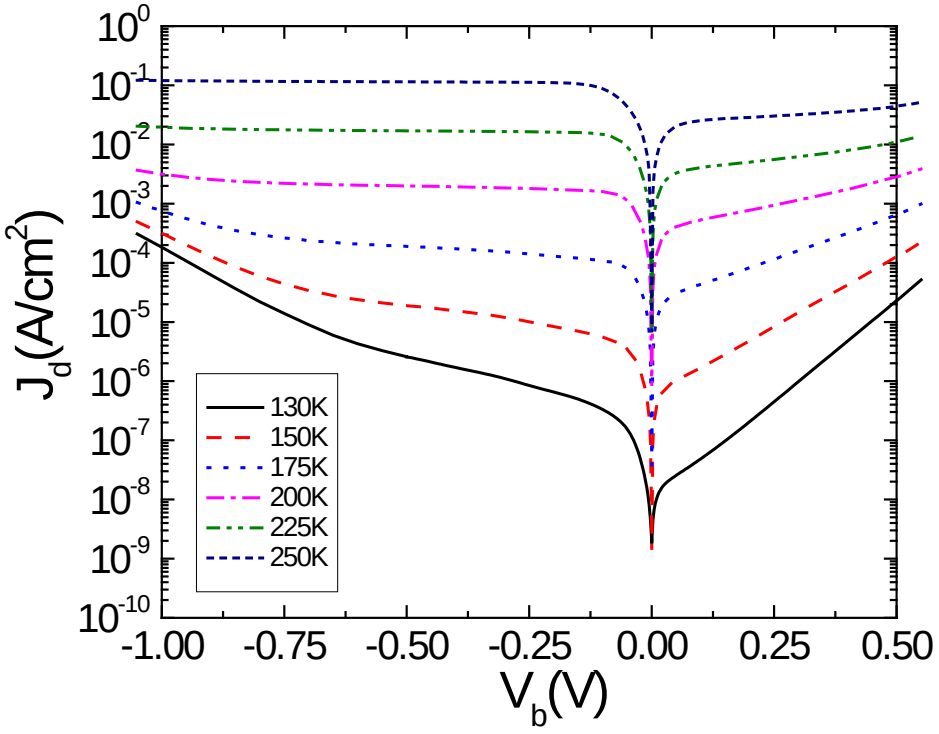

Figure 6. Measured dark current density vs. applied bias in the temperature range T = 130 – 250 K as indicated.

6. DISCUSSION

In summary, we extended the cut-off wavelength λ_c of bulk InAsSb nBn detectors to λ_c = 4.6 μm at T = 200 K by incorporating series of single InSb monolayer into InAsSb absorber. Detectors with 2μm thick absorber showed a temperature independent quantum efficiency $QE^m \approx 0.45$ for back-side illumination without antireflection coating. The dark current density was $j_d = 5 \times 10^{-6}$ A/cm^2 at T = 150K, and increased to $j_d = 2 \times 10^{-3}$ A/cm^2 at T = 200 K.

7. ACKNOWLEDGEMENTS

The research described in this publication was carried out at the Jet Propulsion Laboratory, California Institute of Technology, under a contract with the National Aeronautics and Space Administration

REFERENCES

[1] A. M. White, 'Infrared detectors', USA Patent 4,679,063 (1987).
[2] S. Maimon and G. W. Wicks, Applied Physics Letters **89** (15), 151109 (2006).
[3] P. Klipstein, Proc. SPIE **6940**, 69402U-2 (2008).
[4] A. Rogalski, '*New Ternary Alloy Systems for Infrared Detectors'*, SPIE, Bellingham, Washington, 1994, p. 84.
[5] A. Soibel, D. Z. Ting, C. J. Ting, A. M. Fisher, L. Hoglund, S. A. Keo and S. Gunapala, Applied Physics Letters 109, 103505 (2016).

[6] D. Donetsky, S. P. Svensson, L. E. Vorobjev, and G. Belenky, *Appl. Phys. Lett.* **95**, 212104 (2009).
[7] J. S. Blakemore, Semiconductor Statistics. New York, NY, USA: Dover, 1987.
[8] L. Hogland, D, Z-Y. Ting, A. Soibel, C. J. Hill, A. M. Fisher, S. A. Keo, and S. D. Gunapala, IEEE Photonics Technology Letters **27**(23), 2492-2495 (2015).
[9] A. Soibel, C. J. Hill, S. A. Keo, L. Hoglund, R. Rosenberg, R. Kowalczyk, A. Khoshaklagh, A. Fisher, D. Z.-Y. Ting and S. Gunapala, Applied Physics Letters **105**, 023512 (2014).
[10] D. Z. Ting, A. Soibel, L. Hoglund, C. J. Hill, S. A. Keo, A. Fisher and S. Gunapala, J. of E. Matt., DOI: 10.1007/s11664-016-4633-z (2016).